Harmonic Modeling and Analysis of Series-Parallel Compensated IPT Systems with an Inductive Filter

Chenwen Cheng, Ting Chen, Xiaoman Cui, Yuan Liu, Sheng Zhang, and Chris Mi, *Fellow, IEEE*

***Abstract*— In the series-parallel (S-P) compensated inductive power transfer (IPT) system for the electric vehicle (EV) charging application, an inductive filter is required after the rectifier on the secondary side to avoid the large charging current surge when the diodes conduct. This paper proposes a harmonic modeling method for the S-P compensated IPT systems with an inductive filter where both the fundamental and higher-order harmonics are considered. Compared to the well-known fundamental harmonic approximation (FHA) method, a more accurate description can be obtained by constructing the circuit model at different harmonics, especially in a strongly coupled case. The zero-voltage switching (ZVS) condition is derived, which shows that a larger load current will cause the power switches to lose ZVS. A larger coupling coefficient will help increase the ZVS range. The output DC voltage will drop slightly due to the high order harmonics, which is different from the FHA method where the output voltage is constant regardless of the load. Experimental results are provided to validate the effectiveness of the proposed harmonic modeling method of the S-P compensated IPT system.**

***Index Terms*— inductive power transfer (IPT), S-P, harmonic modeling, inductive filter, zero voltage switching (ZVS).**

I. Introduction

As the inductive power transfer (IPT) technology is getting mature, it has been widely used to charge electric vehicles (EV) [1], consumer electronic devices [2], autonomous underwater vehicles (AUV) [3], gate drivers of power electronic switches in multilevel converters [4, 5], etc. Without any physical contact, IPT technology provides more convenience and modernity when charging EVs, which has received more and more attention [6].

Since the primary and secondary coils are separated in the EV charging scenario, a large amount of magnetic flux leakage is unavoidable, which leads to a loose coupling coefficient compared to the conventional transformer. To enhance the power transfer capability of the IPT system [7], different compensation methods such as series-series (S-S) [8], series-parallel (S-P) [9], parallel-series (P-S) [10], and parallel-parallel (P-P) [10], LCC-LCC [11], LCL-LCL [12], LCC-S [13] and S-LCC [14] are employed where additional compensation capacitors or inductors are used in the primary and secondary sides.

Usually, a DC power supply is required for the load. Thus, a rectifier and the corresponding filtering circuit are used on the secondary side to transform the received AC power into a stable DC form. There are mainly two different kinds of filtering circuits in the IPT system, namely the capacitive filter and the inductive filter as shown in Fig. 1. For some compensation methods such as the S-S and LCC-LCC topologies, the capacitive filter in Fig. 1(a) can be used after the rectifier where a DC link capacitor C_f is directly connected across the output of the rectifier to obtain a stable output [8, 12]. However, for other compensation methods such as the S-P topology that has a capacitor C_p connected in parallel with the rectifier, the capacitive filter is no longer suitable because C_p will be connected in parallel with the DC-link capacitor C_f when the diodes conduct, and a large charging current will be generated. The current surge may damage the diode and generate a large amount of harmonic current in the circuit. The lifetime of C_f will be shortened because of the current harmonics especially when electrolytic capacitors are used [15]. To solve this problem, an inductor L_f can be inserted between the rectifier and the DC-link capacitor [16]. Thus, an inductive filter is formed. The influence of the inductive filter and capacitive filter on the system analysis is different. In the capacitive filter, a square wave voltage is generated before the rectifier, the amplitude of which is equal to the DC-link voltage. The IPT system with a capacitive filter such as the SS or LCL topologies has been well analyzed in the existing publications while the system with an inductive filter deserves deeper analysis. If the inductive filter is adopted, usually a large filtering inductor is used, so that the current flowing through the inductor can be regarded as

Manuscript received xxxx; revised xxxx; accepted xxxx. This work was supported by the State Key Laboratory of Advanced Power Transmission Technology under Grant No. GEIRI-SKL-2022-004. (*Corresponding author: Chris Mi.*)

C. Cheng and X. Cui are with Southeast University, Nanjing, Jiangsu 210018, China (email: chenwen_cheng@seu.edu.cn; 213190925@seu.edu.cn).

T. Chen is with the State Key Laboratory of Reliability and Intelligence of Electrical Equipment, Hebei University of Technology, Tianjin 300130, China (email:mia_tingchen@outlook.com)

Y. Liu and S. Zhang are with State Key Laboratory of Advanced Power Transmission Technology (State Grid Smart Grid Research Institute Co., Ltd.), Beijing 102200, China (email: liuyuan@geiri.sgcc.com.cn; zhangsheng@geiri.sgcc.com.cn).

C. Mi is with the San Diego State University, San Diego, CA 92182 USA (e-mail: mi@ieee.org).

constant. When the diodes in the rectifier conduct, a square wave current will be generated before the rectifier. Thus, the analysis method for the capacitive filter is not suitable for the inductive filter. The S-P topology adopts only one capacitor on both the primary and secondary sides, which has a simpler structure. Therefore, The S-P topology is taken as an example in this paper to investigate the operating mechanism of an IPT system with an inductive filter. The proposed modeling and analysis method can be easily extended to other IPT systems with an inductive filter such as the S-SP topology or those with a capacitive filter such as the S-S topology.

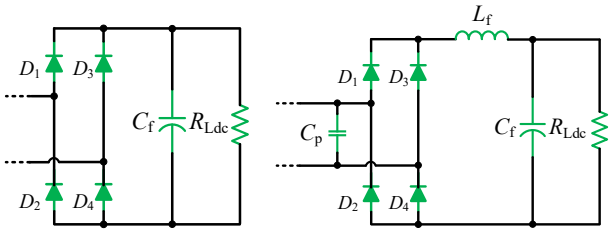

(a) Capacitive filter (b) Inductive filter

Fig. 1. Two different filters used for the IPT system.

Because of the frequency selective characteristic of the IPT system with compensation circuits, the fundamental harmonic approximation (FHA) method is widely used to analyze the system where only the fundamental voltage and current components are considered while high-order harmonics are neglected. The FHA method is accurate when the coupling coefficient is small [17]. However, in some applications, the coupling coefficient can be very large. For example, when charging autonomous guided vehicles (AGV), the distance between the chassis and the ground is only in the tens of mm, and can even drop to a few mm when fully loaded [17, 18]. The coupling coefficient will be close to 1. Then higher-order harmonics cannot be neglected and the FHA method is not precise enough to describe the system performance.

In [19], a modeling method of the S-P compensated IPT system was provided based on the differential equations in the time domain. However, the resonant condition in [19] is different from the commonly used one which can generate a constant voltage output [20]. Moreover, the differential equation method is sophisticated and unintuitive. Especially when the circuit order is high, it is difficult to solve the differential equations to obtain an analytical solution. Thus, a simpler modeling method with a straightforward physical meaning should be established. In [17], a harmonic modeling method was proposed for the capacitive filter-based IPT system. But it does not apply to the inductive filter-based IPT system. This paper will discover more in-depth features of the inductive filter-based IPT system with the proposed harmonic modeling method. Compared with the differential equation-based modeling method, the harmonic modeling method appears to be more intuitive because it is easy to know how the harmonic components vary in such a system by looking at the harmonic circuit. Some different conclusions will be pointed out in this paper.

Thus, a harmonic modeling method for the S-P compensated IPT system with an inductive filter is established in this paper. Not only the fundamental component but also higher-order harmonics in the voltages and currents are considered. Thus, a more accurate model of the IPT system can be obtained as described in section II. Based on the derived harmonic model, detailed analysis such as the ZVS condition of the metal oxide semiconductor field-effect transistors (MOSFETs) in the inverter, the output voltage variation due to the harmonics, the system efficiency is conducted in section III. Section IV provides experimental results to validate the proposed harmonic modeling method. Section V concludes the whole paper.

II. Harmonic Modeling

A. System Description

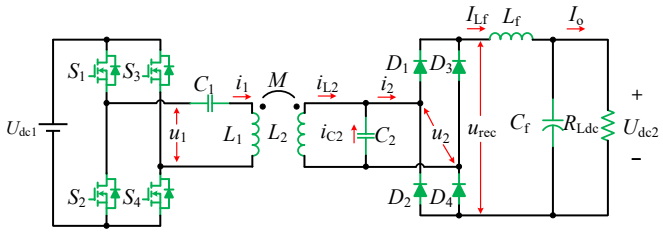

Fig. 2. S-P compensated IPT system with an inductive filter.

As shown in Fig. 2, in the S-P compensated IPT systems, two coils, L_1 and L_2, form an inductive link between the primary and secondary sides. A capacitor C_1 is connected in series with L_1 while C_2 is connected in parallel with L_2. A full-bridge inverter consisting of four MOSFETs, S_1, S_2, S_3, and S_4, is used to generate a high-frequency square wave voltage source u_1 from the DC voltage source U_{dc1}. On the secondary side, four diodes, D_1, D_2, D_3, and D_4, constitute a full bridge rectifier, which transforms the received AC voltage into DC voltage. Since C_2 is connected in parallel with the rectifier, an inductive filter consisting of a filtering inductor L_f and a capacitor C_f is adopted to obtain a stable DC output voltage U_{dc2} as explained above.

In Fig. 2, i_1, i_2, i_{L2}, and i_{C2} are the current flowing through L_1, the rectifier, L_2, and C_2 respectively. The positive directions are defined in Fig. 2. u_2 represents the voltage across the rectifier. u_{rec} is the output voltage of the rectifier. R_{Ldc} is the DC load. I_{Lf} and I_o are the currents flowing through L_f and R_{Ldc} respectively. Usually, the filtering inductor L_f is large so that I_{Lf} can be regarded as constant [19]. As a result, the current i_2 flowing into the rectifier is a square wave when different diodes conduct. Since voltage U_{dc2} across C_f is stable, I_{Lf} is equal to I_o. Fig. 3 shows the waveforms of u_1 and i_2, both of which are square wave signals, and u_1 delays i_2 by a phase angle φ. At instant 0, i_2 changes from negative to positive. The amplitudes of u_1 and i_2 are U_{dc1} and I_o respectively. Then u_1 and i_2 can be rewritten into the Fourier series form as,

$$u_1 = \frac{4}{\pi} U_{dc1} \sum_{n=1,3,5...}^{\infty} \frac{1}{n} \sin(n\omega_0 t - n\varphi) = \sum_{n=1,3,5...}^{\infty} u_{1,n} \tag{1}$$

$$i_2 = \frac{4}{\pi} I_o \sum_{n=1,3,5...}^{\infty} \frac{1}{n} \sin(n\omega_0 t) = \sum_{n=1,3,5...}^{\infty} i_{2,n} \tag{2}$$

where $u_{1,n}$ and $i_{2,n}$ represent the n^{th} order harmonic components

in u_1 and i_2 respectively.

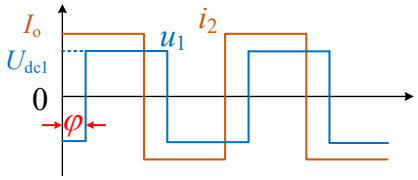

Fig. 3. Theoretical waveforms of the input voltage u_1 and output current i_2.

M is the mutual inductance between L_1 and L_2. Then the coupling coefficient k between L_1 and L_2 can be defined as,

$$k = M/\sqrt{L_1 \cdot L_2} \tag{3}$$

The switching angular frequency of the inverter is selected as the resonant angular frequency ω_0, which is defined as [9, 10, 20],

$$\omega_0^2 = 1/(L_2 \cdot C_2) = 1/[(L_1 - M^2/L_2) \cdot C_1] \tag{4}$$

B. Fundamental Harmonic Modeling

The FHA method is widely used to analyze the IPT system where only the fundamental harmonic is considered while the high-order harmonics are neglected. The fundamental harmonic modeling of the S-P compensated IPT system has already been established in [9]. The derivation process is not repeated here. Only some important equations and conclusions are given to facilitate the analysis.

When (4) is met, the fundamental components of the input current $i_{1,1}$ and output voltage $u_{2,1}$ can be calculated as.

$$i_{1,1} = \lambda i_{2,1} \tag{5}$$

$$u_{2,1} = \lambda u_{1,1} \tag{6}$$

where $\lambda = L_2/M$. It can be seen that $i_{1,1}$ and $u_{2,1}$ depend on $i_{2,1}$ and $u_{1,1}$ respectively. Thus, a constant voltage output regardless of the load can be obtained when the FHA method is adopted. It is also mentioned in [9] that if the resonant condition in (4) is met, zero phase angle (ZPA) can be realized from the primary side. Thus, no reactive power is generated.

C. Higher-order Harmonic Modeling

In order to establish the high-order harmonic model of the S-P compensated IPT system, Fig. 2 can be simplified as Fig. 4 where the mutual inductance model of the two coupled coils is used. It needs to be pointed out that the mutual inductance model of a pair of coupled inductors is not restricted to only the 1:1 turns ratio scenario. The superposition principle can be used to help analyze this circuit where u_1 and i_2 are applied to the circuit respectively. Then the circuit current or voltage will be the sum of the current or voltage generated when u_1 and i_2 act separately.

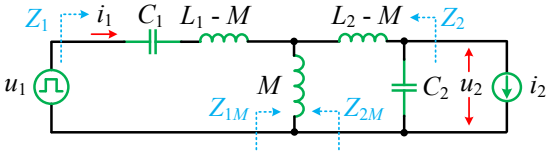

Fig. 4. Simplified model of the S-P compensated IPT system.

In Fig. 4, Z_1 and Z_2 are the impedance seen from the source u_1 and i_2 respectively. Z_{1M} and Z_{2M} are the equivalent impedances seen from the primary and secondary mutual inductance sides. The four impedances at the n^{th} (n = 3, 5, 7,…) order harmonic frequency can be calculated as,

$$Z_{1M,n} = jn\omega_0 M[1 - \frac{n^2}{(n^2-1)\lambda}] \tag{7}$$

$$Z_{1,n} = jn\omega_0 M \cdot \frac{1}{\lambda} \cdot (\frac{1}{k^2} - \frac{1/k^2 - 1}{n^2} - \frac{n^2}{n^2 - 1}) \tag{8}$$

$$Z_{2M,n} = jn\omega_0 M(1 - \frac{n^2\lambda}{n^2/k^2 + 1 - 1/k^2}) \tag{9}$$

$$Z_{2,n} = jn\omega_0 M \cdot \lambda \cdot \frac{(n^2-1)(1-1/k^2)}{(1/k^2-1)(n^2-1)^2 - n^2} \tag{10}$$

When only $u_{1,n}$ is excited, the current $i_{1p,n}$ and voltage $u_{2p,n}$ can be calculated as,

$$\begin{cases} i_{1p,n} = u_{1,n}/Z_{1,n} \\ u_{2p,n} = i_{1p,n} \cdot Z_{1M,n} \cdot \dfrac{1/(jn\omega_0 C_2)}{jn\omega_0(L_2 - M) + 1/(jn\omega_0 C_2)} \end{cases} \tag{11}$$

The subscript "p" means the current or voltage is generated by the primary voltage source u_1. Submitting (7) and (8) into (11), $i_{1p,n}$ and $u_{2p,n}$ in time domain can be simplified as,

$$\begin{cases} i_{1p,n}(t) = \dfrac{-\lambda(n^2-1)}{(1/k^2-1)(n^2-1)^2 - n^2} \cdot \dfrac{4U_{dc1}}{\pi R_b} \cdot \cos(n\omega_0 t - n\varphi) \\ u_{2p,n}(t) = -\dfrac{4U_{dc1}}{\pi} \cdot \dfrac{\lambda n}{(1/k^2-1)(n^2-1)^2 - n^2} \sin(n\omega_0 t - n\varphi) \end{cases} \tag{12}$$

where $R_b = \omega_0 M$.

When only $i_{2,n}$ is excited, the current $i_{1s,n}$ and voltage $u_{2s,n}$ can be calculated as,

$$\begin{cases} u_{2s,n} = -i_{2,n} \cdot Z_{2,n} \\ i_{1s,n} = \dfrac{-u_{2s,n}}{Z_{2M,n} + jn\omega_0(L_2 - M)} \cdot \dfrac{Z_{2M,n}}{1/(jn\omega_0 C_1) + jn\omega_0(L_1 - M)} \end{cases} \tag{13}$$

The subscript "s" means the current and voltage are generated by the secondary current source i_2. Submitting (9) and (10) into (13), $i_{1s,n}$ and $u_{2s,n}$ can be further simplified as,

$$\begin{cases} u_{2s,n}(t) = -\dfrac{\lambda(n^2-1)(k^2-1)}{(1/k^2-1)(n^2-1)^2 - n^2} \cdot \dfrac{4I_o R_b}{\pi k^2} \cdot \cos(n\omega_0 t) \\ i_{1s,n}(t) = -\dfrac{\lambda n}{(1/k^2-1)(n^2-1)^2 - n^2} \cdot \dfrac{4I_o}{\pi} \cdot \sin(n\omega_0 t) \end{cases} \tag{14}$$

Thus, $i_{1,n}$ and $u_{2,n}$ can be calculated as,

$$\begin{aligned} i_{1,n}(t) &= i_{1p,n}(t) + i_{1s,n}(t) \\ &= -\frac{\lambda n}{(1/k^2-1)(n^2-1)^2 - n^2} \cdot \frac{4}{\pi} \cdot I_b \cdot \\ &\quad [\frac{n^2-1}{n}\cos(n\omega_0 t - n\varphi) + \gamma_1 \sin(n\omega_0 t)] \end{aligned} \tag{15}$$

$$u_{2,n}(t)=u_{2p,n}(t)+u_{2s,n}(t)$$
$$=-\frac{\lambda}{(1/k^2-1)(n^2-1)^2-n^2}\cdot\frac{4U_{dc1}}{\pi}\cdot \quad (16)$$
$$[n\sin(n\omega_0 t-n\varphi)+\gamma_1(n^2-1)(1-1/k^2)\cos(n\omega_0 t)]$$

where I_b and γ_1 are the base current value and normalized output current respectively, which can be calculated as,

$$\begin{cases} I_b = U_{dc1}/R_b \\ \gamma_1 = I_0/I_b \end{cases} \quad (17)$$

In (17), I_b is the base current value and depends on U_{dc1} and the resistor base value R_b.

When deriving (15) and (16), n is assumed to vary from 3 to infinity. However, when n=1, (15) and (16) are equal to (5) and (6) respectively. Thus, the range of n in (15) and (16) can be extended to {1, 3, 5, …}.

With $u_{2,n}$ in (16), the n^{th} order harmonic component of i_{C2} as shown in Fig. 2 can be calculated as,

$$i_{C2,n}(t)=-C_2\,du_{2,n}(t)/dt$$
$$=\frac{n}{(1/k^2-1)(n^2-1)^2-n^2}\cdot\frac{4U_{dc1}}{\pi R_b}\cdot[n\cos(n\omega_0 t-n\varphi) \quad (18)$$
$$+\gamma_1(n^2-1)(1/k^2-1)\sin(n\omega_0 t)]$$

Then current i_{L2} flowing through L_2 can be calculated as,

$$i_{L2,n}(t)=i_{2,n}(t)-i_{C2,n}(t)$$
$$=-\frac{n}{(1/k^2-1)(n^2-1)^2-n^2}\cdot\frac{4U_{dc1}}{\pi R_b}\cdot[n\cos(n\omega_0 t-n\varphi) \quad (19)$$
$$+\frac{\gamma_1[(1/k^2-1)(n^2-1)+n^2]}{n^2}\sin(n\omega_0 t)]$$

III. System Analysis

A. Calculation of Phase Angle φ

In (15) and (16), the phase angle φ is unknown, which should be determined first. It needs to be pointed out that when i_2 changes from negative to positive or positive to negative, voltage u_2 across the rectifier will cross zero. $u_2(t)$ can be written as,

$$u_2(t)=\sum_{n=1,3,5...}^{\infty}u_{2,n}(t) \quad (20)$$

According to Fig. 3, t = 0 is one of the zero-crossing instant of $u_2(t)$, which means,

$$u_2(0)=\sum_{n=1,3,5...}^{\infty}u_{2,n}(0)=0 \quad (21)$$

Eq. (21) is a nonlinear equation of φ. It is difficult to get the analytical solution of φ. The numerical solution of φ can be calculated instead. According to (16), the amplitude of $u_{2,n}$ gradually reduces to zero as the harmonic order n increases. Thus, higher-order harmonics in u_2 have smaller influence on the value of φ. When n is large enough, $u_{2,n}$ can be neglected for calculating φ. Fig. 5 shows the variation of φ when the highest harmonic order considered in u_2 increases where k = 0.8 and γ_1 = 0.5. When only the fundamental harmonic is considered, φ is equal to 0 degree, which is consistent with the result in (6). When the highest harmonic order is larger than 800, φ converges to 14.26. Thus, the highest harmonic order can be chosen as 800, which ensures enough accuracy.

Fig. 6 shows the variation of φ with the increasing coupling coefficient k. It can be found that with a larger k or normalized output current γ_1, the phase angle φ increases. Since u_2 and i_2 have the same zero-crossing point, u_2 is also ahead of u_1 by an angle of φ when considering the harmonics in u_2, which depends on k and γ_1.

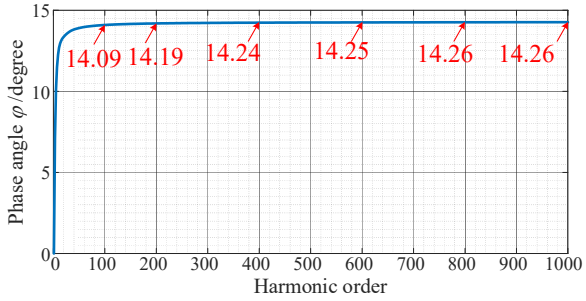

Fig. 5. Variation of φ with the increasing harmonic order (k = 0.8 and γ_1 = 0.5).

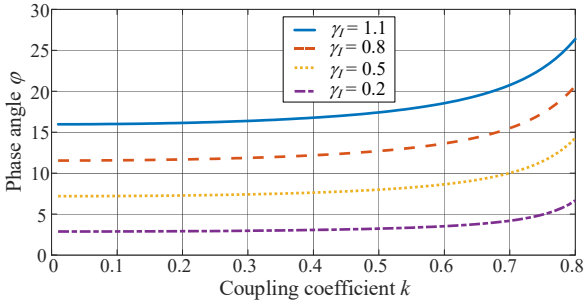

Fig. 6. Variation of φ with the increasing coupling coefficient k.

B. ZVS Condition

The IPT system usually requires a high switching frequency to ensure high efficiency and low volume. To ensure the safe operation of the inverter, ZVS is essential for minimizing the heat generation inside the MOSFETs. In the full bridge inverter, the inverter current i_1 should lag u_1 to some extent to completely discharge the parasitic output capacitor of the MOSFET. Usually, the MOSFET's output capacitance is small. When neglecting the output capacitance, the critical condition to achieve ZVS is that i_1 is crossing zero when u_1 changes from negative to positive. Thus, the following condition should be met,

$$i_1(\frac{\varphi}{\omega_0})=\sum_{n=1,3,5...}^{\infty}i_{1,n}(\frac{\varphi}{\omega_0})=0 \quad (22)$$

Based on the phase angle φ obtained in (21) and Fig. 6, the inverter output current $i_1(\varphi/\omega_0)$ at instant φ/ω_0 can be calculated as shown in Fig. 7. In Fig. 7, $i_1(\varphi/\omega_0)$ is divided by I_b to get the normalized value. It can be seen from Fig. 7 that when the normalized output current γ_1 increases, the normalized inverter output current also increases and changes from negative to positive. Thus, the MOSFETs in the inverter will lose ZVS

when the load current is too large. Moreover, if the coupling coefficient k becomes larger, the output current range where ZVS is ensured will also be wider.

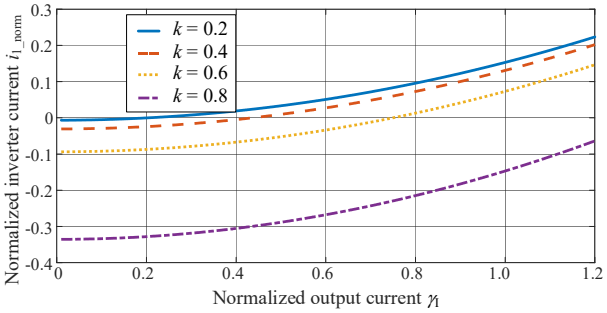

Fig. 7. Normalized $i_1(\varphi/\omega_0)$ with the increasing γ_1 ($\lambda = 0.5$).

In order to obtain the critical normalized load current γ_1 where $i_1(\varphi/\omega_0)$ is zero, eq. (22) should be solved. In (22) two variables are unknown, i.e. φ and γ_1. Combining (21) and (22), an equation set is formed to solve φ and γ_1. The variations of φ and γ_1 against the increasing coupling coefficient k is shown in Fig. 8. If k becomes larger, the critical φ and γ_1 will be larger to realize ZVS of the MOSFETs.

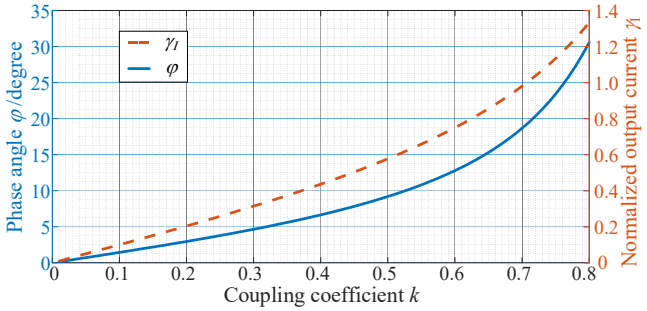

Fig. 8. Phase angle φ and γ_1 to achieve ZVS with different coupling coefficients k.

C. Total Harmonic Distortion (THD) Analysis

With the harmonic components of i_1, i_{L2} , i_{C2} and u_2 in (15), (19), (18) and (16), the THD of them can be calculated by using the following equations,

$$THD_{i1} = \sqrt{\sum_{n=3,5,7...}^{\infty} I_{1\_n}} \Big/ I_{1\_1} \tag{23}$$

$$THD_{iL2} = \sqrt{\sum_{n=3,5,7...}^{\infty} I_{L2\_n}} \Big/ I_{L2\_1} \tag{24}$$

$$THD_{iC2} = \sqrt{\sum_{n=3,5,7...}^{\infty} I_{C2\_n}} \Big/ I_{C2\_1} \tag{25}$$

$$THD_{u2} = \sqrt{\sum_{n=3,5,7...}^{\infty} U_{2\_n}} \Big/ U_{2\_1} \tag{26}$$

where I_{1_n}, I_{L2_n}, I_{C2_n} and U_{2_n} ($n = 1, 3, 5, \ldots$) are the root mean square (RMS) value of the n^{th} harmonics in i_1, i_{L2}, i_{C2} and u_2 respectively.

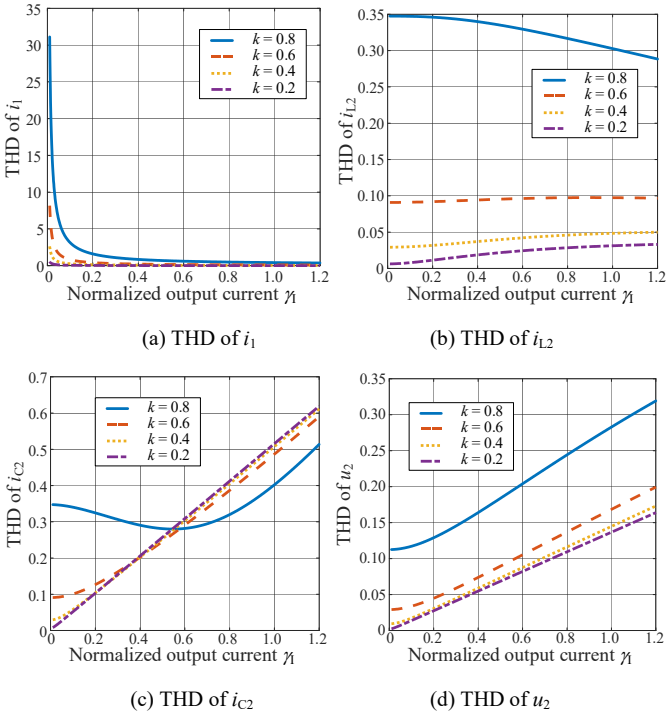

Fig. 9. THDs of i_1, i_{L2}, i_{C2}, and u_2.

Fig. 9 shows the THDs of i_1, i_{L2}, i_{C2}, and u_2 when the normalized output current γ_1 is increasing with different coupling coefficients k. For i_1, the THD is large at a light load while the THD will become smaller at a heavy load. With a larger k, the harmonics in i_1 becomes larger, which is similar to the conclusions in [17]. When k is small, the THD of i_{L2} is almost constant when γ_1 varies. When k becomes larger, i_{L2}'s THD decreases gradually as shown in Fig. 9(b). The THD of i_{C2} increases as γ_1 is growing in a loosely coupled system. When the magnetic coupling becomes stronger (k = 0.8), the THD of i_{C2} decreases first, then grows again as γ_1 increases as shown in Fig. 9(c). The THD of u_2 increases with the growing normalized output current γ_1 and the coupling coefficient k as can be seen from Fig. 9(d). Both the THD of i_{L2} and u_2 are always very small during the whole operating range, which means i_{L2} and u_2 are nearly sinusoidal.

D. AC-to-AC Efficiency

According to (16) and (2), the n^{th} order output power can be calculated as,

$$P_{o,n} = \frac{8U_{dc1}I_o}{\pi^2} \cdot \frac{\lambda}{n^2 - (1/k^2 - 1)(n^2 - 1)^2} \cdot \cos(n\varphi) \tag{27}$$

Compared to the coil's resistance, the capacitor's resistance is small and can be neglected. Assuming that r_1 and r_2 are the resistances of L_1 and L_2, the power generated in r_1 and r_2 because of the n^{th} order current harmonic $i_{1,n}$ and $i_{L2,n}$ are as follows,

$$\begin{cases} P_{L1,n} = |I_{1\_n}|^2 \cdot r_1 \\ P_{L2,n} = |I_{L2\_n}|^2 \cdot r_2 \end{cases} \tag{28}$$

Thus, the AC-to-AC efficiency of the S-P compensated IPT system can be approximately calculated as,

$$\eta=\frac{\sum_{n=1,3,5...}^{\infty} P_{o,n}}{\sum_{n=1,3,5...}^{\infty}(P_{o,n}+P_{L1,n}+P_{L2,n})}\times 100\% \tag{29}$$

Fig. 10 shows the variation of the maximum achievable efficiency with different coupling coefficients k when the quality factor of both L_1 and L_2 are 200. The solid curve is the maximum achievable efficiency when using the FHA method while the dashed line is the maximum achievable efficiency when considering the high order harmonics. It can be seen that if FHA is used to model the S-P compensated IPT system, the maximum achievable efficiency will increase with a larger k. However, the maximum achievable efficiency will grow first then drop as k increases if the proposed harmonic model is adopted.

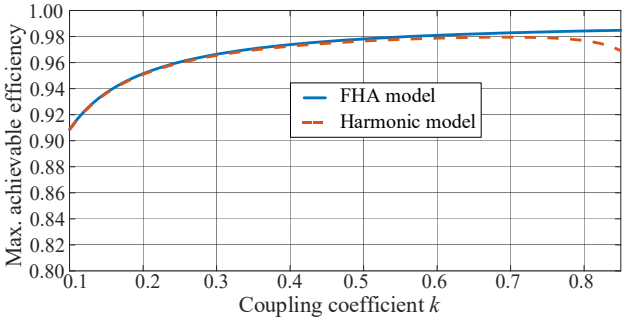

Fig. 10. Variation of the maximum achievable coil-to-coil efficiency.

E. Output Voltage

In order to calculate the output voltage U_{dc2}, a voltage equation on the output rectifier can be written as,

$$u_{rec}=L_f\, dI_{Lf}/dt+U_{dc2} \tag{30}$$

Due to the voltage-second balance of the filter inductor L_f, the output voltage U_{dc2} can be calculated as,

$$U_{dc2}=\frac{\omega_0}{\pi}\int_{t=0}^{\pi/\omega_0} u_{rec}(t)\cdot dt \tag{31}$$

It needs to be noted that in the period $[0, \pi/\omega_0]$, $u_{rec}(t)$ is equal to $u_2(t)$. Thus, submitting (16) into (31) the following equation can be obtained,

$$U_{dc2}=\frac{8\lambda U_{dc1}}{\pi^2}\cdot\sum_{n=1.3.5...}^{\infty}\left[-\frac{\cos(n\varphi)}{(1/k^2-1)(n^2-1)^2-n^2}\right] \tag{32}$$

If the FHA method is used to model the S-P compensated IPT system, U_{dc2} can be simplified as,

$$U_{dc2\_FHA}=8\lambda U_{dc1}/\pi^2 \tag{33}$$

In this case, a constant output DC voltage independent of the load is obtained. Based on (32), the output DC voltage variation using the proposed harmonic model is shown in Fig. 11 where U_{dc2} is divided by (33) to get a normalized value. As the load current grows, U_{dc2} decreases gradually. It is because the load current variation will affect the phase angle φ. Then U_{dc2} will be affected too according to (32). Moreover, with a higher coupling coefficient k, U_{dc2} will have a larger drop because of the high order harmonics. Thus, the output DC voltage U_{dc2} is no longer constant when considering high order harmonics, which is different from the conclusion when the FHA method is used to analyze the system. It needs to be pointed out that the power loss caused by the coil's resistance or the power device's voltage drop is not considered here, which will lead to a further output DC voltage drop. It should be noted when designing such a system because the load voltage may not reach the expected value.

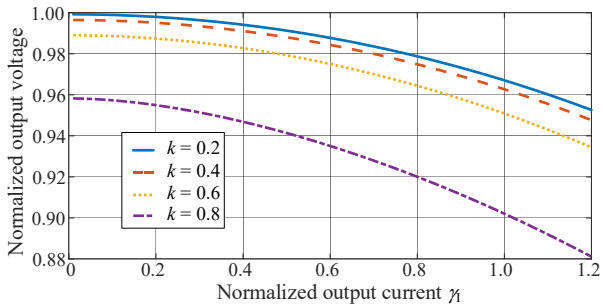

Fig. 11. Output DC voltage characteristics.

IV. Experimental Validation

A. Experimental Setup

An experimental platform of the S-P compensated IPT system was built as shown in Fig. 12. An inverter consisting of four SiC MOSFETs (C2M0080120D) is used to generate a high-frequency AC power source for the IPT system. On the secondary side, a rectifier consisting of four SiC diodes (IDW30G65C5) transforms the AC to DC. An inductive filter is used to obtain a stable DC output for the electric load. Power analyzer WT1800 is adopted to analyze the system power and efficiency. In the experiment, four different scenarios with different coupling coefficients are compared by changing the distance between the transmitting pad and the receiving pad. The parameters in different scenarios are listed in Table I where the switching frequency of the inverter is 85 kHz.

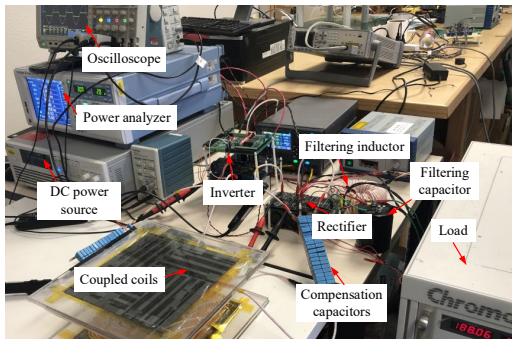

Fig. 12. Experimental platform of an S-P compensated IPT system.

TABLE I. Experimental Parameters

k	0.24	0.43	0.59	0.80
U_{dc1} /V	60	100	100	100
L_1 /μH	49.02	51.31	54.73	65.32
L_2 /μH	47.60	49.96	53.62	63.45

M /μH	11.39	21.54	31.95	51.32
λ	4.18	2.32	1.68	1.24
C_1 /nF	75.8	83.4	98.3	147.1
C_2 /nF	73.7	70.2	65.3	55.3
L_f /μH	730	730	730	730
C_f /uF	3300	3300	3300	3300

B. *Experimental Results*

Fig. 13 shows the waveforms of u_1, i_1, u_2 and i_2 when $k = 0.43$ and $\lambda = 2.32$. The calculated i_1 and u_2 using (15) and (16) are also shown in Fig. 13 for comparison. It can be seen that the measured voltages and currents match the calculated values well, which verifies the correctness of the proposed modeling method. The current profiles depend on many factors like the coupling coefficient k, the load current and so on. For example, In Fig. 13, when $\gamma_1 = 0.174$, the waveform of i_1 is highly distorted. Although in other figures the currents are more sinusoidal, it can still be seen that harmonic components exist. The FHA method is no longer precise enough to describe the system performance. The best way is to use the quantitative analysis method proposed in this paper to obtain the accurate results.

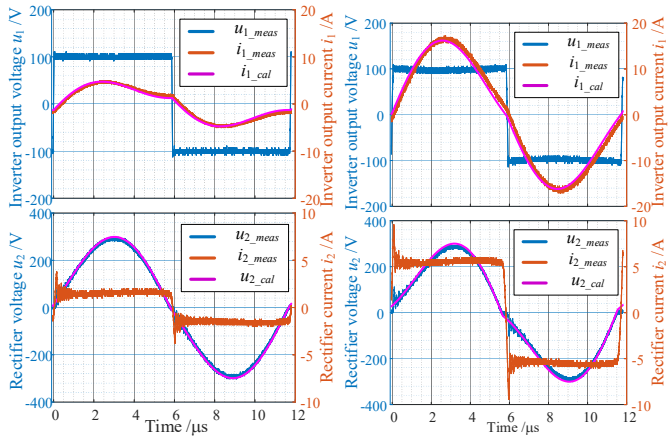

(a) $\gamma_1 = 0.174$ (b) $\gamma_1 = 0.61$

Fig. 13. Experimental waveforms ($k = 0.43$, $\lambda = 2.32$).

When the output current is small ($\gamma_1 = 0.174$), ZVS can be realized for the MOSFETs in the inverter as shown in Fig. 13(a). Increasing the output current to $\gamma_1 = 0.61$, the critical condition is achieved where the zero-crossing instant of i_1 is the same as that of u_1. If γ_1 continues increasing, hard switching will happen, which will generate higher switching loss and may damage the MOSFETs. The variation of the critical normalized load current γ_1 that can achieve ZVS against the coupling coefficient k is shown in Fig. 14. A larger critical γ_1 comes with a larger k, which is consistent with the calculated values. It can be seen that the measured values are always above the calculated line using the proposed harmonic model. This is mainly because of the dead-zone inserted between the turning-on driving signals of the two MOSFETs in the same bridge arm to avoid the shoot-through problem. The dead-zone causes the voltage crossing-zero instant ahead of the current crossing-zero instant, which helps realize the ZVS even at the critical condition. Although there exists some error between the measured values and the calculated values, the MOSFETs can work safely according to the design guideline based on the harmonic modeling method because the real ZVS range is larger than the calculated one.

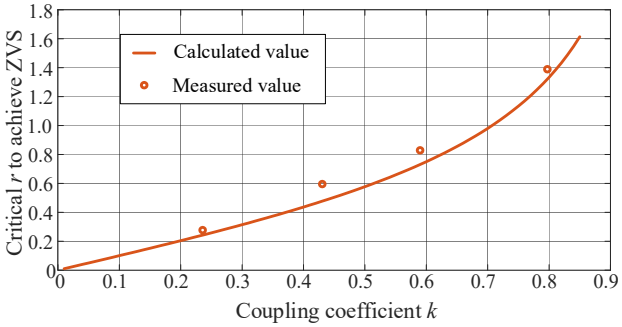

Fig. 14. Critical load current variation versus the coupling coefficient.

Fig. 15 shows the calculated and measured THD values of currents and voltages when the coupling coefficient $k = 0.8$. The solid line indicates the calculated value while the circle represents the measured values. It can be seen that the measured values match the calculated values well. Fig. 16 shows the harmonic distribution of i_{C1} when $k = 0.8$ and $\gamma_1 = 0.12$. The largest harmonic component is the 3rd one. The magnitude of the harmonic gradually decreases as the harmonic order increases.

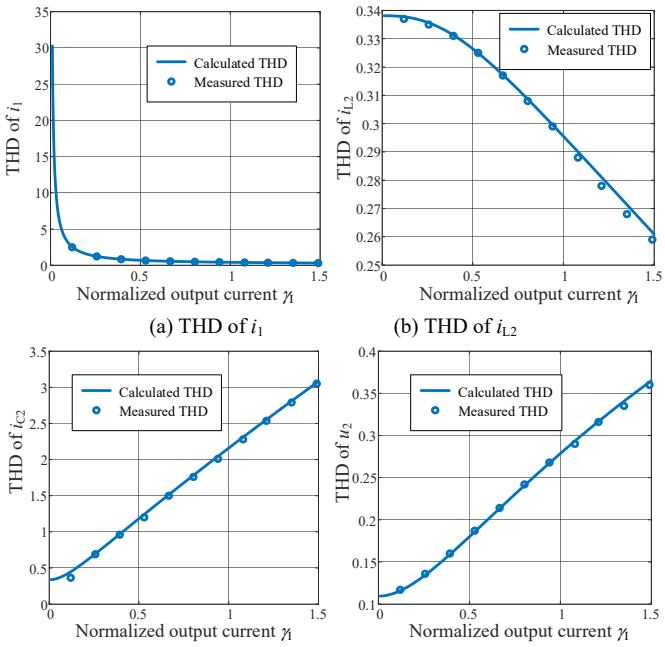

(a) THD of i_1 (b) THD of i_{L2}

(c) THD of i_{C2} (d) THD of u_2

Fig. 15. Calculated and measured THD when $k = 0.8$.

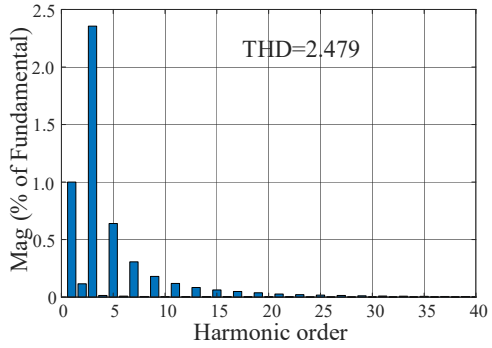

Fig. 16. Harmonic distribution of i_{C1} when $k = 0.8$ and $\gamma_I = 0.12$.

The system efficiency variations versus the increasing output power under different coupling conditions are shown in Fig. 17. The measured data is the complete DC-DC efficiency, which includes the loss of the inverter and rectifier. The maximum system efficiencies at the coupling coefficients of 0.24, 0.43, 0.59 and 0.80 are 0.94, 0.96, 0.964, and 0.958 respectively. It can be seen that when the coupling coefficient increases to 0.8, the maximum efficiency drops a little, which is because of the harmonic loss as analyzed above.

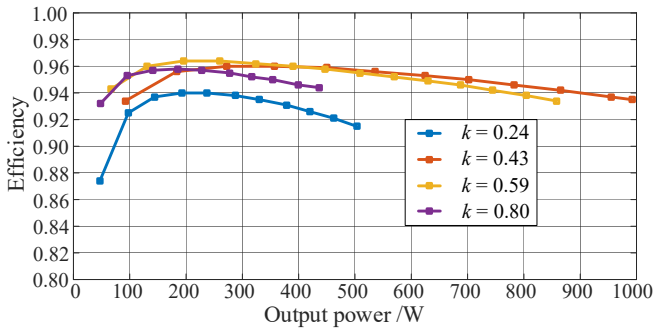

Fig. 17. System efficiency variations with different coupling coefficients.

Fig. 18 depicts the variation of the system efficiency when the output power increases when k = 0.8. The quality factor of the coil is measured as 450. The blue curve is the calculated coil-to-coil efficiency when using the conventional FHA method, while the red curve is the calculated efficiency when using the proposed harmonic model. It can be seen that the efficiency calculated using the harmonic model is slightly lower than that calculated using the FHA method because of the harmonic loss. The dots represent the measured efficiency. Since the MOSFETs, diodes, and the filtering inductor cause additional loss, the measured efficiency is lower than the calculated values.

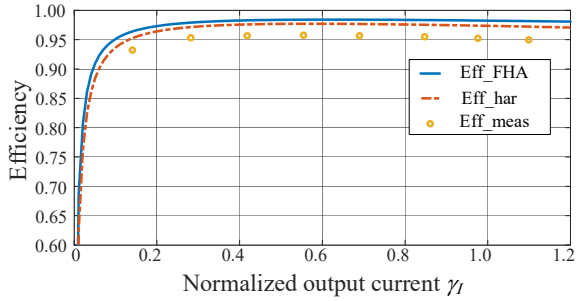

Fig. 18. System efficiency variation when $k = 0.8$.

Fig. 19 illustrates the output power variation with increasing load currents when k = 0.8. The solid line is the calculated output power using the proposed harmonic model in the paper while the circle dot represents the measured output power in the experiment. The measured power basically matches the calculated value.

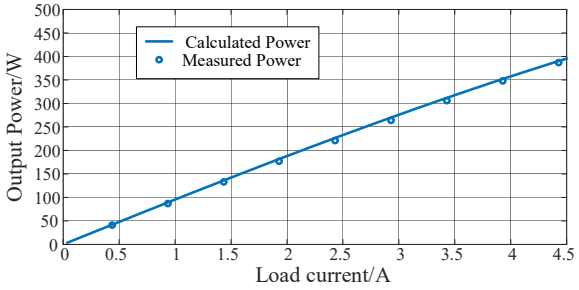

Fig. 19. Output power variation when $k = 0.8$.

Fig. 20 shows the power loss distribution when the input power is 409W and the coupling coefficient is 0.8, where (a) shows the calculated power loss distribution and (b) shows the measured values. The main power loss lies in the filter inductor because a larger inductor was adopted to filter out the load current harmonics. Because the power loss is small, there exist errors in the measuring results. Basically, the measured power losses match the calculated values.

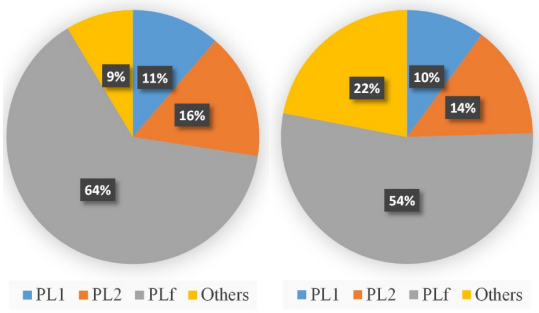

(a) (b)

Fig. 20. Power loss distribution when the input power is 409W and k is 0.8: (a) Calculated power loss distribution; (b) Measured power loss distribution.

The variation of the output DC voltage V_{dc2} as the output current grows is shown in Fig. 21. Considering voltage drops on the filtering inductor's parasitic resistance and the diodes in the rectifier, eq. (32) can be revised as,

$$U_{dc2} = \frac{8U_{dc1}}{\pi^2} \cdot \sum_{n=1.3.5...}^{\infty} [-\frac{\lambda \cdot \cos(n\varphi)}{(1/k^2 - 1)(n^2 - 1)^2 - n^2}] - I_o R_{Lf} - 2V_F \quad (34)$$

where V_F is forward voltage of the diode and R_{Lf} is the parasitic resistance of L_f. When the output current increases, the output voltage U_{dc2} calculated using the FHA method remains constant, while the measured U_{dc2} decreases gradually. Compared with the calculated values using the proposed harmonic model, the voltage drop in the experiment is larger, which is because of the diodes' forward voltage drop, the voltage drop on the filtering inductor, and the power loss in the coils and ferrite.

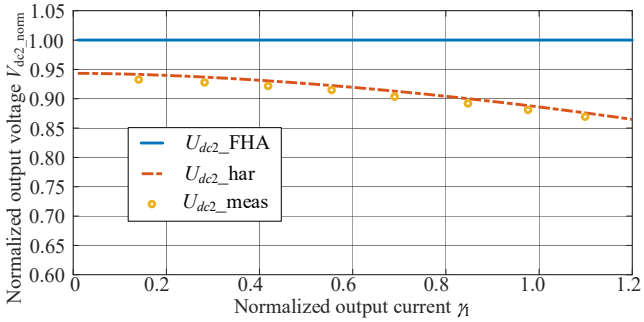

Fig. 21. Output DC voltage variation (k = 0.8).

V. Conclusion

This paper proposed a harmonic modeling method for the S-P compensated IPT system with an inductive filter for the EV application. Not only the fundamental harmonic component but also higher-order harmonics are considered in this method. Thus, a more precise description of the S-P compensated IPT system can be obtained. A detailed derivation process is provided to help determine the amplitude of any order harmonic. Compared to the differential equation modeling method in the time domain, the proposed harmonic modeling method is more intuitive. Different from the FHA method, some new conclusions can be drawn from the proposed harmonic model.

1) In a weakly-coupled IPT system, the FHA method is widely adopted in the analysis and design process of an IPT system with a satisfactory accuracy. But errors will increase when the coupling coefficient becomes larger.

2) It is found that ZVS of the MOSFETs in the inverter may be lost if the load current is too large. Increasing the coupling coefficient k will help enlarge the ZVS range, which is different from Ref. [17]. The proposed harmonic modeling method provides guidelines to ensure ZVS of the MOSFETs when designing the S-P compensated IPT system.

3) The maximum achievable efficiency does not increase all the time as k increases. When k is too large such as charging the AGV or high power EV where the transmitting and receiving pads are close, the maximum achievable efficiency will drop because of the high order harmonics.

4) The output DC voltage decreases gradually with an increasing load even the system loss is neglected. The conclusion that a constant output voltage can be obtained when using the FHA method is not accurate.

Such a complete harmonic modeling method provides a deeper insight into the S-P compensated IPT system and helps design a more efficient inductive EV charging system, which can also be used to model other IPT systems with an inductive filter such as the S-SP system. Although the above conclusions can also be observed using simulation tools, the harmonic model is more profound and provides precise description of the system, which provides quantitative guidelines when designing the system. The derivation process seems complex, but the results and conclusion are direct and concise, which can be employed easily in the design process.

References

[1] S. Li and C. C. Mi, "Wireless power transfer for electric vehicle applications," *IEEE J. Emerg. Sel. Topics. Power Electron.*, vol. 3, no. 1, pp. 4–17, Mar. 2015.

[2] S. Y. R. Hui, W. W. C. Ho, "A new generation of universal contactless battery charging platform for portable consumer electronic equipment," *IEEE Trans. Power Electron.*, vol. 20, no. 3, pp. 620–627, May 2005.

[3] E. Gati, G. Kampitsis, S. Manias, "Variable frequency controller for inductive power transfer in dynamic conditions," *IEEE Trans. Power Electron.*, vol. 32, no. 2, pp. 1684–1696, Feb. 2017.

[4] C. Cheng, F. Lu, Z. Zhou, W. Li, C. Zhu, H. Zhang, Z. Deng, X.Chen, and C. Mi, "Load-independent wireless power transfer system for multiple loads over a long distance," *IEEE Trans. Power Electron*., vol. 34, no. 9, pp. 9279–9288, Sept. 2019.

[5] C. Liu, F. Deng, Q. Heng, X. Cai, R. Zhu and M. Liserre, "Crossing Thyristor Branches-Based Hybrid Modular Multilevel Converters for DC Line Faults," *IEEE Trans. Ind. Electron.*, vol. 68, no. 10, pp. 9719-9730, Oct. 2021.

[6] Z. Zhang, H. Pang, A. Georgiadis, C. Cecati, "Wireless power transfer – an overview," *IEEE Trans. Ind. Electron.*, vol. 66, no. 2, pp. 1044-1058, Feb. 2019.

[7] S. Y. R. Hui, W. Zhong, C. K. Lee, "A critical review of recent progress in mid-range wireless power transfer," *IEEE Trans. Power Electron*., vol. 29, no. 9, pp. 4500–4511, Sept. 2014.

[8] E. Gati, G. Kampitsis, S. Manias, "Variable frequency controller for inductive power transfer in dynamic conditions," *IEEE Trans. Power Electron*., vol. 32, no. 2, pp. 1684–1696, Feb. 2017.

[9] C. Cheng, Z. Zhou, W. Li, Z. Deng, and C. C. Mi, "A power relay system with multiple loads using asymmetrical coil design," *IEEE Trans. Ind. Electron.*, Early Access.

[10] V. B. Vu, D. H. Tran, W. Choi, "Implementation of the constant current and constant voltage charge of inductive power transfer systems with the double-sided LCC compensation topology for electric vehicle battery charge application," *IEEE Trans. Power Electron*., vol. 33, no. 9, pp. 7398–7410, Sept. 2018.

[11] S. Li, W. Li, J. Deng, T. D. Nguyen, and C. C. Mi, "A double-sided LCC compensation network and its tuning method for wireless power transfer," *IEEE Trans. Veh. Technol*., vol. 64, no. 6, pp. 2261–2273, Jun. 2015.

[12] Y. Yao, Y. Wang, X. Liu, F. Lin, and D. Xu, "A novel parameter tuning method for a double-sided LCL compensated WPT system with better comprehensive performance," *IEEE Trans. Power Electron*., vol. 33, no. 10, pp. 8525–8536, Oct. 2018.

[13] C. Cheng, W. Li, Z. Zhou, Z. Deng, and C. C. Mi, "A load-independent wireless power transfer system with multiple constant voltage outputs," *IEEE Trans. Power Electron*., vol. 35, no. 4, pp. 3328–3331, Apr. 2020.

[14] R. Mai, Y. Chen, Y. Zhang, N. Yang, G. Gao, and Z. He, "Optimization of the passive components for an S-LCC topology-based WPT system for charging massive electric bicycles," *IEEE Trans. Ind. Electron.*, vol. 65, no. 7, pp. 5497-5508, Jul. 2018.

[15] K. Nishizawa, J. I. Itoh, A. Odaka, A. Toba, and H. Umida, "Current harmonic reduction based on space vector PWM for DC-link capacitors in three-phase VSIs operating over a wide range of power factor," *IEEE Trans. Power Electron*., vol. 34, no. 5, pp. 4853–4867, May 2019.

[16] M. Ishihara, K. Umetani, E. Hiraki, "Elucidation of quasi-duality between series-series and series-parallel topologies of resonant inductive coupling wireless power transfer systems," in *Proc. IEEE Power Electron. Drive Syst. Conf.*, Honolulu, HI, USA, 2017, pp. 674–679.

[17] F. Lu, Y. Zhang, H. Zhang, C. Zhu, L. Diao, M. Gong, W. Zhang, and C. Mi, "A low-voltage and high-current inductive power transfer system with low harmonics for automatic guided vehicles," *IEEE Trans. Veh. Technol*., vol. 68, no. 4, pp. 3351–3360, Apr. 2019.

[18] F. Lu, H. Zhang, C. Zhu, L. Diao, M. Gong, W. Zhang, C. C. Mi, "A tightly coupled inductive power transfer system for low-voltage and high-current charging of automatic guided vehicles," *IEEE Trans. Ind. Electron.*, vol. 66, no. 9, pp. 6867-6875, Sept. 2019.

[19] Y. Zhang, Z. Yan, T. Kan, X. Zeng, S. Chen, and C. C. Mi, "Modeling and analysis of a strongly coupled series-parallel-compensated wireless power transfer system," *IEEE J. Emerg. Sel. Topics. Power Electron*., vol. 7, no. 2, pp. 1364–1370, Jun. 2019.

[20] B. K. Kushwaha, G. Rituraj, P. Kumar, P. Bauer, "Mathematical model for the analysis of series-parallel compensated wireless power transfer

system for different misalignments," *IET Circuits Devices Syst.,* vol. 13, no. 7, pp. 970–978, Oct. 2019.

Chenwen Cheng received his B.S. and Ph.D. degrees from Zhejiang University, Hangzhou, China, in 2012 and 2017, respectively, all in electrical engineering. From 2018 to 2021, he was a postdoc researcher in San Diego State University, San Diego, California, USA. He is now with Southeast University. His research interests include motor control, renewable power generation, and wireless power transfer technologies.

Ting Chen received the B.S., M.S., and Ph.D. degrees from the China University of Mining and Technology, Beijing, China, in 2015, 2017, and 2022, respectively. From November 2019 to November 2021, she was a joint Ph.D. student with the Department of Electrical and Computer Engineering, San Diego State University, San Diego, CA, USA. She is currently an assistant professor with the Department of Electrical Engineering and State Key Laboratory of Reliability and Intelligence of Electrical Equipment, Hebei University of Technology. Her current research interests include wireless power transfer technologies, modeling and control of switching converters.

Xiaoman Cui received her B.E. degree from Southeast University, Nanjing, China, in 2023 in electrical engineering. She is now pursuing the M.S. degree at University of California, Los Angeles, California, USA. Her research interests include power electronics and electric machines.

Yuan Liu received the B.S. and M.S. degrees in electrcial engineering from Xi'an Jiaotong University, Xi'an, China, in 2006 and in 2009 respectively. She is now with State Grid Smart Grid Research Institute Co.,.Ltd. Her research interests include the topology and energy supply system of DC breaker.

Sheng Zhang received the B.S. degree in electrical engineering from Dalian Maritime University, Dalian, China, in 2005, and the M.S. degree from Xi'an Jiaotong University, Xi'an,China, in 2008, and the Ph.D. degree from Wuhan University, Wuhan, China, in 2022. He is now with State Grid Smart Grid Research Institute Co.,.Ltd. His research interests include HVdc converter, hybrid dc breaker, and dc cable.

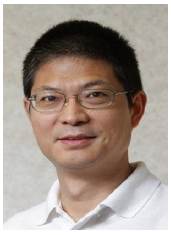

Chris Mi (S'00–A'01–M'01–SM'03–F'12) received the B.S.E.E. and M.S.E.E. degrees in electrical engineering from Northwestern Polytechnical University, Xi'an, China, and the Ph.D. degree in electrical engineering from the University of Toronto, Toronto, Ontario, Canada, in 1985, 1988, and 2001, respectively.

He is a Professor and chair of electrical and computer engineering and the Director of the Department of Energy (DOE) -funded Graduate Automotive Technology Education (GATE) Center for Electric Drive Transportation, San Diego State University, San Diego, USA. Prior to joining SDSU, he was with University of Michigan, Dearborn from 2001 to 2015.